Microscopic Pathway for the Medium-Chain Fatty Acyl CoA Dehydrogenase Catalyzed Oxidative Half-Reaction: Changes in the Electronic Structures of Flavin and CoA Derivatives during Catalysis‡

Jeffrey K. Johnson, N. Ravi Kumar, and D. K. Srivastava*

Biochemistry Department, North Dakota State University, Fargo, North Dakota 58105

Received June 1, 1993; Revised Manuscript Received July 23, 1993®

ABSTRACT: In a previous communication, we demonstrated that the medium-chain fatty acyl CoA dehydrogenase (MCAD) catalyzed conversion of 3-indolepropionyl CoA (IPCoA) to *trans*-3-indoleacryloyl CoA (IACoA) proceeds via the formation of an intermediary species X that possesses the electronic properties of reduced flavin and highly conjugated CoA product. Since the steady-state turnover of the enzyme-catalyzed dehydrogenation reaction precisely matches with the rate of formation of X [Johnson, J. K., & Srivastava, D. K. (1993) *Biochemistry 32,* 8004–8013], the latter species appeared to be the likely site for the transfer of electrons to external electron acceptors (e.g., ferricenium hexafluorophosphate, $FcPF_6$). To probe the microscopic pathway for the oxidative half-reaction, we employed a sequential mixing stopped-flow technique utilizing IPCoA as the enzyme substrate and $FcPF_6$ as the electron acceptor. The time-dependent changes in absorption at 450, 415, and 367 nm were measured upon mixing $FcPF_6$ with previously mixed and aged solutions of MCAD–FAD + IPCoA in the stopped-flow syringes. The kinetic traces show an increase ($1/\tau_1$) followed by a decrease ($1/\tau_2$) in absorption at 450 and 415 nm, and a lag (corresponding to the time regime of $1/\tau_1$) followed by an increase in absorption ($1/\tau_2$) at 367 nm. The relaxation rate constants ($1/\tau$'s) thus measured remain unaffected, with variations in the aging time; however, the amplitudes of these phases increase up to the aging time of 5 s, after which the amplitudes attain maxima. For an aging time of 5 s, $1/\tau_1$ and $1/\tau_2$ show a linear and a hyperbolic dependence on the $FcPF_6$ concentration, respectively. These, coupled with the complementary studies involving butyryl CoA as a nonchromophoric substrate for this enzyme, lead us to propose the following sequence of events during the MCAD-catalyzed oxidative half-reaction: (1) The enzyme-catalyzed oxidative half-reaction proceeds via the formation of a collision complex between X and $FcPF_6$ during the fast ($1/\tau_1$) relaxation phase. (2) The reduced flavin moiety of X is oxidized via (rapid) transfer of electrons to $FcPF_6$ within the collision complex, without formation of a detectable (metastable) flavin semiquinone intermediate. (3) The transfer of electrons is accompanied by changes in the electronic structures of both the flavin and IACoA moieties within the enzyme–IACoA complex. The electronic structure of this newly formed complex is exactly the same as that formed upon isomerization of the MCAD–FAD–IACoA complex [Johnson, J. K., Wang, Z. X., & Srivastava, D. K. (1992) *Biochemistry 31,* 10564–10575]. (4) The electronically perturbed flavin and IACoA species revert back to their normal structures during the slow ($1/\tau_2$) relaxation phase. This step is followed by the dissociation of IACoA from the enzyme site to promote the subsequent round of catalytic cycle.

Medium-chain fatty acyl CoA dehydrogenase (MCAD)[1] catalyzes the oxidation of medium chain fatty acyl CoA substrates, leading to the formation of *trans*-enoyl CoA during the first step of the mitochondrial fatty acid β-oxidative pathway (Beinert, 1963). The "flavin" cofactor of the enzyme is reduced by the transfer of two electrons (in the form of a hydride ion) from the β position of the substrate molecule, with concomitant oxidation of the substrate (Ghisla et al., 1984). The repetitive turnover of the enzyme is maintained via the transfer of electrons from the reduced flavin moiety to a number of suitable electron acceptors; the physiological electron acceptor of this enzyme is the electron-transferring flavoprotein (ETF) (Crane & Beinert, 1956; Lehman & Thorpe, 1990). Due to the ease of isolation, as well as the distinct spectroscopic signals associated with the various forms of the flavin cofactor (viz., fully oxidized, semiquinone, and fully reduced), this enzyme has been the subject of intense mechanistic investigations over the past several years (Ikeda et al., 1985; Auer & Frerman, 1980; Pohl et al., 1986; Schopfer et al., 1988). This aspect has been strengthened further by the ability of this enzyme to utilize a variety of aliphatic as well as aromatic (usually at the ω-position) fatty acyl CoA substrates (Knoop, 1904; McFarland et al., 1982, Murfin, 1974).

Recently, we introduced indolepropionyl CoA (IPCoA) as a competent substrate for MCAD, which is converted into an intense chromophoric product, indoleacryloyl CoA (IACoA) with an absorption maximum at 367 nm (ϵ_{367} = 26 500 M^{-1} cm^{-1}) (Johnson et al., 1992):

‡ Journal article no. 2120 of the North Dakota Agricultural Experiment Station. Supported by the American Heart Association, Dakota Affiliate.

* Author to whom correspondence should be addressed.

® Abstract published in *Advance ACS Abstracts,* October 1, 1993.

[1] Abbreviations: MCAD, medium-chain fatty acyl CoA dehydrogenase; IPCoA, 3-indolepropionyl coenzyme A; IACoA, *trans*-3-indoleacryloyl coenzyme A; $FcPF_6$, ferricenium hexafluorophosphate; FAD, flavin adenine dinucleotide; $FADH_2$, reduced flavin adenine dinucleotide; $FADH_{sq}$, flavin adenine dinucleotide semiquinone; EDTA, ethylenediaminetetraacetic acid; RSSF, rapid scanning stopped-flow spectroscopy; ETF, electron transferring flavoprotein.

0006-2960/93/0432-11575$04.00/0

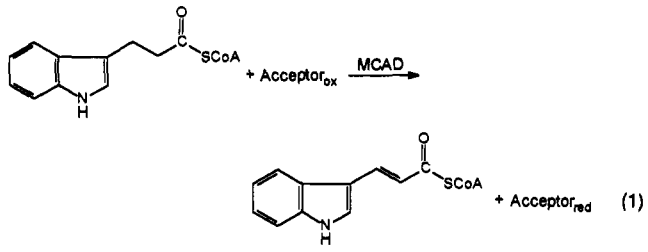

(1)

By utilizing the chromophoric potential of IACoA, we could probe the microscopic environment of the enzyme site. In this endeavor, we noted that the absorption maximum of IACoA is red-shifted upon interaction with either the oxidized or the reduced form of the enzyme. The spectrum of the MCAD–FAD–IACoA complex is characterized by the appearance of two positive bands at 417 and 490 nm and a negative band at 355 nm (Johnson et al., 1992). The magnitude of these spectral changes was found to be a function of the pH of the buffer media. This, coupled with the transient kinetic as well as pH jump studies, led us to propose that the red shift in the IACoA spectrum is caused by the polarization of the carbonyl group under the influence of some electrophilic side chain residue of the protein (Johnson et al., 1992).

Further insights into the structural/functional relationships in MCAD catalysis have been gained from the time-resolved structural changes [via rapid-scanning stopped-flow (RSSF) spectroscopy] during the course of the reductive half-reaction of this enzyme (Johnson & Srivastava, 1993). This approach revealed that the reduction of MCAD–FAD (concomitant with the conversion of IPCoA to IACoA) proceeds via the formation of an intermediary species, X, that is characterized by the absorption spectra of reduced flavin and highly conjugated IACoA species. This latter species exhibits an absorption maximum at 400 nm and is further characterized by the appearance of a broad charge transfer complex band at about 600 nm. Interestingly, the electronic structure of IACoA within X is different from that found in the enzyme–IACoA "colored" complex (denoted as MCAD–FAD*–IACoA** throughout the text), as evidenced by their absorption properties (Johnson et al., 1992).

We and others have noted that the intermediary species (X) formed during the reductive half-reaction decays in the presence of a high concentration of substrate (Schopfer et al., 1988; Johnson & Srivastava, 1993). After a detailed mechanistic analysis utilizing IPCoA as the enzyme substrate, we have proposed the following scheme for the MCAD-catalyzed reductive half-reaction:

$$\text{MCAD–FAD} + \text{IPCoA} \underset{k_s}{\rightleftharpoons} \text{MCAD–FAD–IPCoA} \overset{k_1}{\underset{k_{-1}}{\rightleftharpoons}} \text{X} \overset{k_2}{\underset{k_{-2}}{\rightleftharpoons}}$$

$$\text{MCAD–FADH}_2\text{–IACoA} \overset{K_p^*}{\rightleftharpoons} \text{MCAD–FADH}_2 + \text{IACoA} \quad (2)$$

$$+$$

$$\text{S}$$

$$K_s^* \Big\| \downarrow$$

$$\text{MCAD–FADH}_2\text{–IPCoA}$$

One of the interesting catalytic features of MCAD is that, in addition to catalyzing the normal dehydrogenation reaction in the presence of a variety of "organic" electron acceptors, it also catalyzes an oxidation reaction by utilizing molecular oxygen as the terminal electron acceptor (McFarland et al., 1982; Wang & Thorpe, 1991). The partition between the dehydrogenation and oxidation reactions appears to be dictated by the nature of the substrate (Schopfer et al., 1988; Wang & Thorpe, 1991). The oxidation reaction arises as a result of the conversion of X into the MCAD–$FADH_2$–IACoA complex due to competitive binding of IPCoA (vis-á-vis IACoA) at the MCAD–$FADH_2$ site. This step has been found to limit the rate of the oxidation reaction. However, for the dehydrogenation reaction, the rate limiting step appears to be the formation of X from the MCAD–FAD–IPCoA complex (Johnson & Srivastava, 1993).

Due to the marked instability of X, particularly in the presence of high concentrations of IPCoA, the experimental approach for delineating the oxidative half reaction seemed difficult at first. However, we soon realized that this reaction could be easily performed using a sequential (double) mixing stopped-flow device. As will be elaborated subsequently, this approach allows the immediate production of X, followed by its reaction with the electron acceptor. This, coupled with the spectral properties of the chromophoric species involved during the course of the reaction, has enabled us to delineate the sequence of events occurring during the MCAD-catalyzed oxidative half-reaction.

MATERIALS AND METHODS

Materials. Coenzyme A, glucose oxidase (type VII), and EDTA were purchased from Sigma. 3-Indolepropionic acid and *trans*-3-indoleacrylic acid, used in the synthesis of substrates, were purchased from Aldrich. All other reagents were analytical reagent grade.

Methods. The CoA derivatives of 3-indolepropionic acid (IPCoA) and *trans*-3-indoleacrylic acid (IACoA) were synthesized and purified according to the procedures described previously (Johnson et al., 1992). Medium chain fatty acyl CoA dehydrogenase (MCAD) was purified in our laboratory as described previously (Johnson et al., 1992).

All experiments were performed in a standard 50 mM potassium phosphate buffer (pH 7.6) containing 0.3 mM EDTA at 25 °C unless stated otherwise. MCAD was routinely assayed in this buffer utilizing 30 μM octanoyl CoA and 200 μM ferricenium hexafluorophosphate ($FcPF_6$) as described by Lehman et al. (1990). The active enzyme concentration was determined in terms of the flavin content by using an extinction coefficient of 15.4 mM^{-1} cm^{-1} at 446 nm (Thorpe et al., 1979). IPCoA and IACoA concentrations were determined using extinction coefficients of 18.2 mM^{-1} cm^{-1} at 259 nm and 26.5 mM^{-1} cm^{-1} at 367 nm, respectively (Johnson et al., 1992). The $FcPF_6$ concentration was determined spectrophotometrically using an extinction coefficient of 410 M^{-1} cm^{-1} at 617 nm (Lehman et al., 1990). The extinction coefficient of ferrocene was determined by comparing the absorption of an ethanolic solution of ferrocene with $FcPF_6$ at 400 nm. At this wavelength, the extinction coefficients of ferrocene and $FcPF_6$ are equal (Lehman et al., 1990).

Steady-state kinetics and conventional spectral acquisitions were performed on Perkin-Elmer Lambda 3B and Beckman 7400 diode array spectrophotometers. Single-wavelength transient kinetic studies and data analyses were performed on an Applied Photophysics MV-14 sequential mixing stopped-flow system.

The rapid-scanning stopped flow (RSSF) spectrophotometer used in these studies was configured as described previously (Johnson & Srivastava, 1993). The RSSF spectra were smoothed using a convolution approach which performs a least-squares fit to a specified window of data points according to the method of Savitsky and Golay (1964) with the aid of Spectracalc (Galactic Industries Corporation) software. The

number of smothing points was 9–21, depending upon the signal to noise ratio of the RSSF traces.

Sequential Mixing Stopped-Flow Experiments. Sequential mixing stopped-flow experiments were performed on an Applied Photophysics MV-14 stopped-flow system. Syringes A and B contained MCAD–FAD and substrate, respectively. Syringe C contained $FcPF_6$, while syringe D contained buffer. At zero time, syringes A and B were pushed simultaneously, causing the enzyme and substrate to mix in the mixing chamber. After a predetermined age time, precisely controlled by the computer workstation, syringes C and D were simultaneously pushed to allow mixing of all of the reagents in the cuvette. This followed data acquisition at a desired wavelength. The design of mixing circuit was such that the concentrations of solutions A and B were reduced by 25%, whereas the concentration of solution C was reduced only by 50%, of original solution concentrations.

Anaerobic Experiments. Buffers and solutions were made anaerobic by bubbling and degassing in 2 × 15-min cycles with argon scrubbed free of oxygen using an oxytrap (Alltech). Immediately prior to use of these reagents in the rapid-scan or stopped-flow systems, glucose oxidase and glucose were added to concentrations of 30 μg/mL and 0.8 mM, respectively, to remove any traces of oxygen.

Data Analysis. The stopped-flow kinetic traces were analyzed either by the data analysis package provided by Applied Photophysics or by the nonlinear regression analysis software, Enzfitter (BioSoft).

The time-dependent reaction traces were simulated by the numerical integration software "PLOD" [Kahaner, D. K., & Barnet, D. D. Center for Computing and Applied Mathematics, National Institute of Standards and Technology, Gaithersburg, MD], as described by Betts and Srivastava (1991).

RESULTS

A steady-state kinetic investigation of the MCAD-catalyzed dehydrogenation reaction utilizing IPCoA as a substrate and saturating concentration of $FcPF_6$ (200 μM) as the electron acceptor, in 50 mM phosphate buffer (pH 7.6) containing 0.3 mM EDTA, yields K_m (for IPCoA) and k_{cat} values of 10.1 μM and 0.4 s^{-1}, respectively. A comparison of these parameters with the microscopic rate constants for the MCAD-catalyzed reductive half-reaction (eq 2), under identical experimental conditions, reveals that K_m for IPCoA is equal to the dissociation constant for the MCAD–FAD–IPCoA complex (11.5 μM), while k_{cat} is equal to the forward rate constant (0.4 s^{-1}) for the conversion of the latter species to X (Johnson & Srivastava, 1993). These facts, as well as other corroborating evidence (Schopfer et al., 1988; Gorelick et al., 1985), led us to conjecture that X might be a potential site for electron transfer from the enzyme to $FcPF_6$ during the course of the oxidative half-reaction.

To investigate the sequence of events occurring during the reaction of X (produced upon the reaction of MCAD–FAD with IPCoA) with $FcPF_6$, we realized that the following two constraints must be overcome. (1) Due to the unstable nature of X, this species must be generated immediately before the reaction with $FcPF_6$. (2) Since all of the reactants possess overlapping spectral signals, the contribution of the spectral signal of the individual chromophoric species at a particular wavelength must be discerned. Of these, the first constraint was overcome by performing sequential mixing stopped flow experiments (see Materials and Methods, and below). The assignment of absorption changes to individual chromophoric

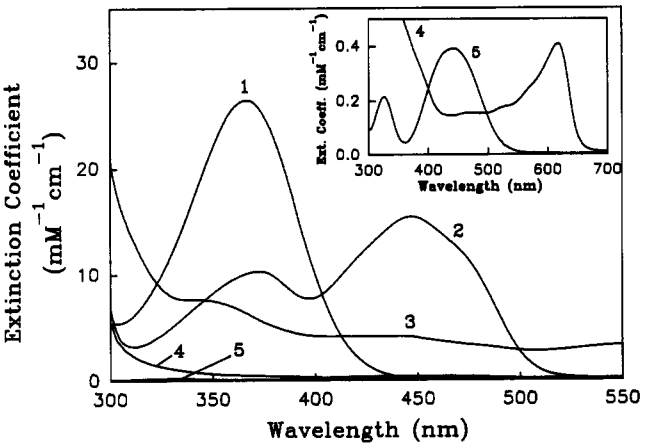

FIGURE 1: UV/vis spectra of IACoA (1), MCAD–FAD (2), MCAD–$FADH_2$ (3), $FcPF_6$ (4), and ferrocene (5) plotted as the extinction coefficient as a function of wavelength. The spectra of all species were recorded in 50 mM potassium phosphate buffer (pH 7.6) containing 0.3 mM EDTA at 25 °C, with the exception of ferrocene in which ethanol was used as the solvent.

species appeared difficult to us at first. To achieve this objective, we decided to examine the spectral properties of all of the chromophoric species utilized or produced during the course of the reaction. In addition, we decided to utilize butyryl CoA as a nonchromophoric substrate to identify signal changes exclusively due to the formation/disappearance of the oxidized flavin. This stratagem was further prompted by the fact that the microscopic pathway for the reductive half-reaction involving IPCoA as the enzyme substrate is identical to that obtained with butyryl CoA (Schopfer et al., 1988; Johnson & Srivastava, 1993).

Spectral Properties of the Participating Chromophoric Species. Figure 1 shows the absorption spectra of IACoA, MCAD–FAD, MCAD–$FADH_2$, $FcPF_6$(ox), and ferrocene (representative of the reduced $FcPF_6$). Due to the extremely low extinction coefficients of IPCoA, butyryl CoA, and crotonyl CoA in the 300–550 nm wavelength region, their absorption contributions have been considered to be negligible. From the spectral data of Figure 1, it is evident that IACoA is the most intense chromophoric species of all of the substrates utilized. Although the absorption spectra of the oxidized and the reduced $FcPF_6$ are different (inset of Figure 1), they are indistinguishable (except in lower wavelength regions) on the extinction coefficient scale of the other chromophoric species. This implies that the reduction of $FcPF_6$ during the initial time regimes of enzyme catalysis would not result in any significant absorption changes above 400 nm. However, in the lower wavelength region, e.g., 367 nm, the absorption changes due to the reduction of $FcPF_6$ would be detectable, particularly when butyryl CoA (nonchromophoric) is utilized as the enzyme substrate.

In addition to the spectral properties of these (stable) chromophoric species, we examined the transient spectral changes during the reductive half-reaction via the rapid-scanning stopped-flow (RSSF) method involving both butyryl CoA and IPCoA as substrates (data not shown). In the case of butyryl CoA, the reaction progress is characterized by a uniform decrease in absorption in all wavelength regions, although the decrease is more pronounced in the absorption maxima of the oxidized flavin (i.e., at 370 and 450 nm). This is in contrast to the changes in the spectral pattern when IPCoA is utilized as the substrate. At initial time regimes, the reduction of the 450-nm flavin band proceeds with a concomitant increase in the absorption band at 400 nm due

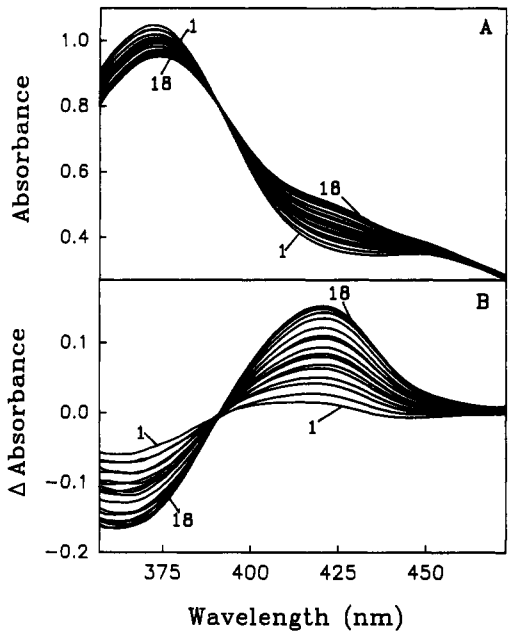

FIGURE 2: Rapid-scanning stopped-flow spectra for the interaction of MCAD–FAD with IACoA. The concentrations of MCAD–FAD (syringe A) and IACoA (syringe B), prior to mixing, were 30 and 40 μM, respectively. The time sequences for the spectral traces (1–18) in panel A range from 0.0086 to 0.396 s. The spectra in panel B are the difference spectra, i.e., spectrum at a given time minus the first spectrum. Other conditions are the same as those given for Figure 1.

to the formation of X (Johnson & Srivastava, 1993). The latter chromophoric band slowly collapses into the absorption band that is more characteristic of the aqueous IACoA (367 nm). These spectral features attest to our earlier contention that the absorption bands at 400 nm (when IPCoA is utilized as the enzyme substrate) must be due to the electronic structures of IACoA within the intermediary complexes and not due to the electronic structures of the flavin moiety.

On the basis of static spectral and single-wavelength stopped-flow studies, we previously proposed that the interaction of MCAD–FAD with IACoA proceeds via two steps (Johnson et al., 1992). The first (fast) step involves the formation of an MCAD–FAD–IACoA "colorless" collsion complex, which is slowly isomerized to an MCAD–FAD*–IACoA** "colored" complex, in which the electronic structures of both flavin and IACoA are drastically perturbed:

$$\text{MCAD–FAD} + \text{IACoA} \rightleftharpoons$$
$$\underset{\text{(colorless)}}{\text{MCAD–FAD–IACoA}} \rightleftharpoons \underset{\text{(colored)}}{\text{MCAD–FAD*–IACoA**}} \quad (3)$$

Since, during the course of the electron-transfer reaction, either (or both) of these species was expected to be formed, we became interested in examining the time-resolved spectral changes for the MCAD–FAD + IACoA interaction reaction. Figure 2 shows the RSSF data for the interaction of MCAD-FAD with IACoA. Note that the reaction progress is characterized by an increase and a decrease in the absorptions at 420 and 360 nm, respectively. This feature is more pronounced in the difference spectrum (Figure 2B), i.e., the spectra at a given time minus the zero time spectrum of Figure 2A. The spectral changes observed herein are consistent with an isosbestic point at 390 nm, suggesting a two-step transition between these enzyme-bound species. This is in agreement with our spectrophotometric titration result that the resultant spectrum of the enzyme–IACoA complex yields a positive peak at 417 nm and a negative peak at 355 nm (Johnson et al., 1992). These spectral changes attest to the fact that the electronic structure of IACoA within the isomerized colored MCAD–FAD*–IACoA** complex is much different from that obtained within the intermediary complex X (Johnson & Srivastava, 1993).

Sequential Mixing Stopped-Flow Studies for the Reaction of X with $FcPF_6$. With the spectral properties of different chromophoric species in mind, we proceeded to investigate the mechanistic pathway for the transfer of electrons from X to $FcPF_6$ by employing a sequential mixing stopped-flow technique (see Materials and Methods). This method allowed us to generate a "nascent" form of X (the magnitude of which was controlled by the aging time) by mixing MCAD–FAD with butyryl/IPCoA via two (A and B) stopped-flow syringes. This was followed by the reaction of X with an excessive concentration of $FcPF_6$ by mixing the latter via the third (C) stopped-flow syringe. Due to technical problems, we have not been able to acquire time-resolved spectra, at this time, during the sequential mixing experiments. Consequently, the reaction progress was monitored at selected wavelengths, viz., 450, 415, and 367 nm. The absorption changes observed at these wavelengths were primarily dominated by the spectra of oxidized flavin, colored form of the MCAD–FAD*–IACoA** species, and aqueous IACoA respectively.

(A) Reaction of Butyryl CoA Generated X with $FcPF_6$. Figure 3 (left panels) shows the double mixing stopped-flow data for the reaction of $FcPF_6$ with the mixed (and aged) solutions of MCAD–FAD plus butyryl CoA (see above) as a function of aging time at the above-mentioned wavelengths. An examination of the time-dependent traces reveals the following: (1) The reaction progress is characterized by an increase ("burst") in absorbance at all wavelengths due to reoxidation of enzyme bound flavin by $FcPF_6$. (2) As the aging time increases, the reaction traces start at lower absorption values, i.e., the absorption at zero time decreases with the increase in aging time. The total absorption changes upon completion of the reaction are thus increased with the increase in the aging time. This is because with an increase in aging time, a higher concentration of MCAD–$FADH_2$ is produced, which is oxidized by $FcPF_6$, resulting in higher amplitudes. The amplitudes of absorption changes (during the burst phase) attain maxima when the aging time reaches 3–5 s. (3) For an aging time of 5 s, the increases in absorption (during the burst phase) at 367, 415, and 450 nm have been found to be 0.0094, 0.016, and 0.034, respectively. The predicted absorption changes at corresponding wavelengths for the complete oxidation of $FADH_2$ (present in X) to FAD under our experimental conditions are 0.012, 0.019, and 0.035, respectively. This prediction is based on the difference in the extinction coefficients of MCAD–FAD and MCAD–$FADH_2$ (Figure 1) and the microscopic rate constants for the formation of X from MCAD–FAD + butyryl CoA (Schopfer et al., 1988). Note the remarkable correspondence between the observed and the predicted absorbance changes during the oxidative half-reaction in Figure 3 (left panels). This is further supported by the observation that the final absorption after the burst phase does not exceed the absorption of the reaction trace obtained for the 20-ms aging time. It can be calculated (Schopfer et al., 1988) that, during this aging time, practically no FAD is reduced to $FADH_2$. (4) The burst phases at all wavelengths are consistent with a single exponential rate law (except for at 367 nm, where the single-exponential phase is followed by a zero-order decrease in absorption). The relaxation rate constants ($1/\tau$) obtained from the best fit of the experimental data (smooth solid lines) at different aging

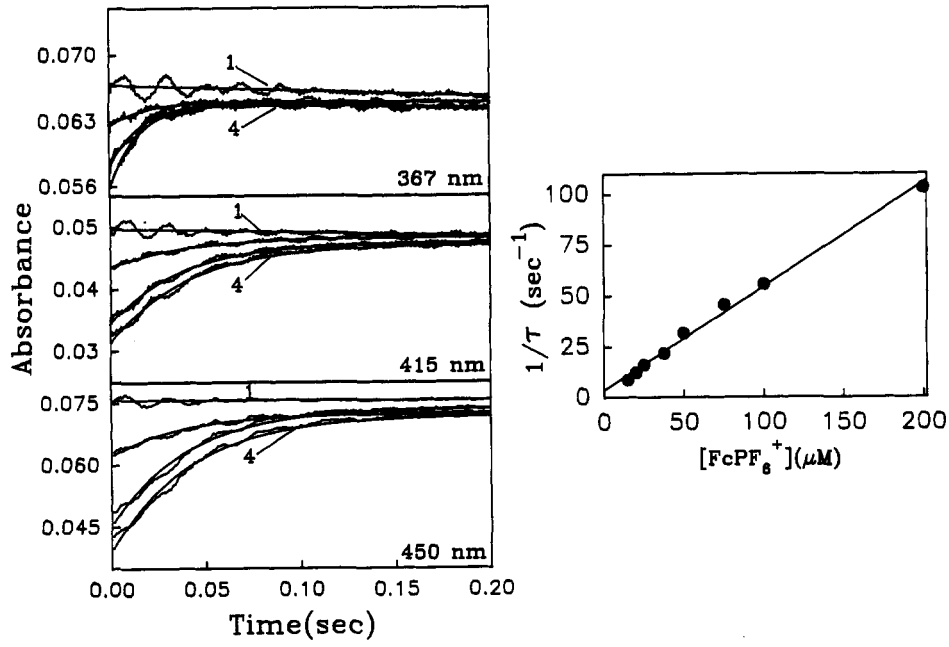

FIGURE 3: Representative stopped-flow traces for the sequential mixing of MCAD–FAD and butyryl CoA with $FcPF_6$ at various aging times and wavelengths. Stopped-flow syringes contained the following: 20 μM MCAD–FAD (syringe A); 200 μM butyryl CoA (syringe B); and 100 μM $FcPF_6$ (syringe C). Traces 1–4 (left panels) correspond to aging times of 0.02, 0.1, 0.5, and 5 s, respectively. Smooth solid lines are the best fit of the experimental data either by single exponential (s^{-1}), by zero order ($\mu M\ s^{-1}$), or by a combination of the two. The calculated rate constants are in the following ranges: 367 nm, 55.13–67.24 s^{-1} and 0.68–2.9 $\mu M\ s^{-1}$; 415 nm, 25.34–27.56 s^{-1}; 450 nm, 24.26–27.77 s^{-1}. Other conditions are the same as those given for Figure 1. The panel on the right side shows the $FcPF_6$ concentration-dependent relaxation rate constant ($1/\tau$) measured at 450 nm at a fixed aging time of 5 s. The concentrations of MCAD–FAD and butyryl CoA (after mixing) were 2.5 and 50 μM, respectively. The x-axis represents the concentration of $FcPF_6$ after mixing. The solid line is the best fit (linear dependence) of the experimental data, with slope and intercept equal to 0.51 $\mu M^{-1}\ s^{-1}$ and 3.70 s^{-1}, respectively.

times vary between 24.26 and 27.77 s^{-1} at 450 nm, 25.34 and 27.56 s^{-1} at 415 nm, and 55.13 and 67.24 s^{-1} at 367 nm. At this time, we do not understand the reason for the 2-fold faster relaxation rate constant at 367 nm (see the Discussion). Also at 367 nm, the burst phase is followed by a zero order decrease in absorption. This zero-order phase has been attributed to the accumulation of reduced $FcPF_6$ (the extinction coefficient of reduced $FcPF_6$ is far different from that of oxidized $FcPF_6$ at 367 nm; see the inset in Figure 1) during initial turnover of the enzyme. The turnover rate of the enzyme calculated from this zero-order phase (2.9 s^{-1}) is similar to that measured under identical experimental conditions (2.24 s^{-1}). (5) In the light of these findings, we are led to conclude that no metastable (red) flavin semiquinone species is generated during the course of the oxidation of enzyme-bound $FADH_2$ to FAD by $FcPF_6$ (see the Discussion). The (red) semiquinone, however, appears when the reaction progress is measured on a longer time scale (data not shown). This is presumably due to the "mutation" reaction between oxidized flavin and reduced $FcPF_6$ (Gorelick et al., 1985; Beckmann & Frerman, 1985). The amplitude of such a mutation reaction decreases when the concentration of the oxidized $FcPF_6$ exceeds that of the reduced $FcPF_6$ (produced during the course of reaction).

Having established that there is only one observed relaxation rate constant ($1/\tau$) for the reaction of X with $FcPF_6$, we investigated the dependence of $1/\tau$ on $FcPF_6$ concentration. As shown in Figure 3 (right panel), $1/\tau$ (measured at 450 nm) demonstrates a linear dependence on $FcPF_6$ concentration, with slope and intercept equal to 0.51 ± 0.02 $\mu M^{-1}\ s^{-1}$ and 3.70 ± 1.40 s^{-1}, respectively. According to the model presented in the Discussion section, the slope is a measure of the association "on rate" constant for the X–$FcPF_6$ complex, whereas the intercept is a measure of the dissociation "off rate" constant of the X–$FcPF_6$ complex multiplied by the equilibrium partition function of the electron transfer step (see eq 11).

(B) Reaction of IPCoA Generated X with $FcPF_6$. In contrast to the uniform pattern of absorbance changes in the experiments shown in Figure 3 (left panels), complementary sequential mixing experiments involving IPCoA as substrate yield unique patterns at individual wavelengths. Figure 4 (left panels) shows the time-dependent absorption changes upon reaction of $FcPF_6$ with the mixed and aged solution of MCAD–FAD plus IPCoA at 450, 415 and 367 nm.

(1) At 450 nm, as the aging time increases, the reaction traces start at progressively lower absorption values, and after 5 s of reaction, they all attain (almost) a constant absorption value. The reaction progress is characterized by two phases: an initial rapid burst in absorbance followed by a slow decay. These two phases are more pronounced when the aging time exceeds 1 s. The kinetic traces are consistent with two relaxation rate constants, $1/\tau_1 > 1/\tau_2$, with average values of 22.0 ± 1.3 and 5.51 ± 1.47 s^{-1}, respectively. The amplitude of $1/\tau_1$ is greater than that of $1/\tau_2$, and both of these amplitudes attain constant values after an aging time of 5 s.

(2) At 415 nm, when the aging time is about 20 ms, an apparent zero-order increase in absorption is noteworthy. This is partly due to steady-state turnover of the enzyme contributed by the tailing absorption peak of IACoA at this wavelength (see Figure 1). As the aging time increases, the reaction traces start at progressively higher absorption values and attain correspondingly higher absorption values after 1 s. The kinetic traces are once again characterized by an initial burst (single-exponential) phase followed by a slow (single-exponential) decay phase, consistent with the two relaxation rate constants ($1/\tau_1 > 1/\tau_2$). Since an increasing zero-order phase is found at 20-ms aging time, all of the kinetic traces have been analyzed (solid line) by two exponentials (increase and decrease) plus

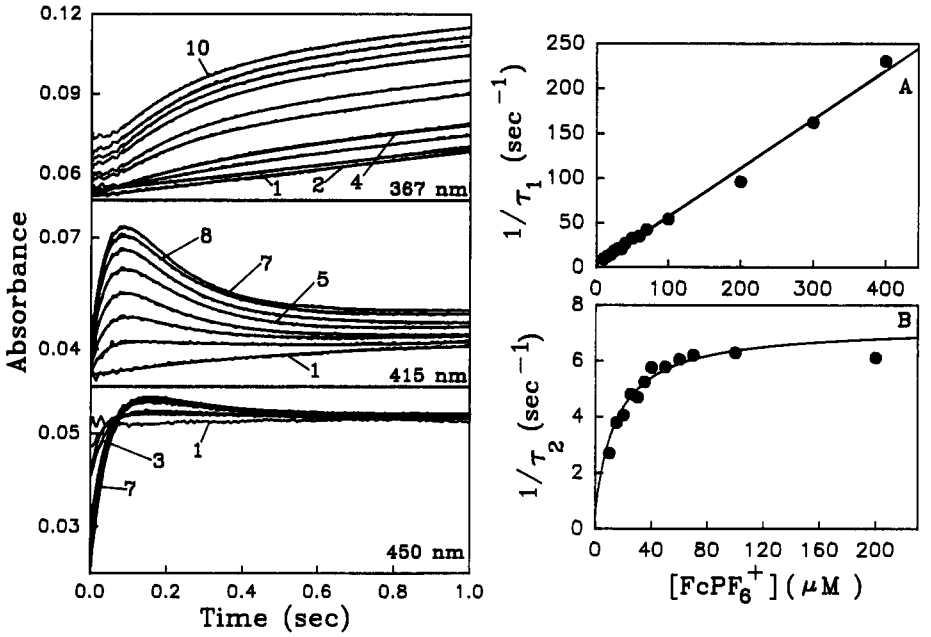

FIGURE 4: Representative stopped-flow traces for the sequential mixing of MCAD–FAD and IPCoA with $FcPF_6$ at various wavelengths and aging times (left panels). Stopped-flow syringes contained the following: 12 μM MCAD–FAD (syringe A); 100 μM IPCoA (syringe B); 100 μM $FcPF_6$ (syringe C). Other conditions are the same as those given for Figure 3. The aging times from different traces in the left panels varied from 0.02 to 15 s. Smooth solid lines are the best fit of the experimental data by double exponential (at 415 and 450 nm), by single exponential at 367 nm (s^{-1}), by zero order (ΔA s^{-1}), or by a combination of these. The calculated rate constants are in the following ranges: 367 nm, $1/\tau_2$ = 2.17–5.2 s^{-1} and zero order = 0.013–0.017 ΔA s^{-1}; 415 nm, $1/\tau_1$ = 21.96–28.29 s^{-1}, $1/\tau_2$ = 1.83–6.63 s^{-1}, and zero order = 0.001–0.006 ΔA s^{-1}; 450 nm, $1/\tau_1$ = 20.31–42.11 s^{-1}, $1/\tau_2$ = 3.74–8.24 s^{-1}, and zero order (trace 1) = 0.001 ΔA s^{-1}. The panels on the right side show $FcPF_6$ concentration-dependent relaxation rate constants ($1/\tau_1$ and $1/\tau_2$) measured at 415 nm at a fixed aging time of 5 s. The MCAD–FAD and IPCoA concentrations after mixing were 1 and 25 μM, respectively. The x-axis represents the concentrations of $FcPF_6$ after mixing. The solid line in right panel A is the best fit (linear dependence) of $1/\tau_1$ versus $FcPF_6$ concentration, with a slope and intercept equal to 0.54 μM^{-1} s^{-1} and 2.68 s^{-1}, respectively. The solid line in right panel B is the best fit of experimental data for a hyperbolic dependence (with offset) for $1/\tau_2$ on $FcPF_6$ concentration, with $1/\tau_2$(max), $1/\tau_2$(min), and $K_{0.5}$ equal to 7.2 s^{-1}, 0.5 s^{-1}, and 15.13 μM, respectively.

a zero-order phase. The average values of $1/\tau_1$, $1/\tau_2$, and the zero-order rate constant from the best fit of the experimental data have been found to be 23.8 ± 1.2 s^{-1}, 5.7 ± 0.7 s^{-1}, and 0.0025 ± 0.002 absorbance change/s, respectively.

(3) Unlike the absorbance changes at 450 and 415 nm, at 367 nm the kinetic traces show a "lag" phase in the time regime corresponding to the increases in the absorptions at 450 and 415 nm. As the aging time increases, the kinetic traces start at progressively higher absorption values. At aging times lower than 200 ms, the initial lag phase is followed by a zero-order increase in absorption. However, at higher aging times, the lag phase is followed by a (slow) burst phase, which conforms to a single-exponential rate law with an average relaxation rate constant of 4.84 ± 0.40 s^{-1}. After the burst phase, a zero-order increase in absorption at 367 nm continues. This zero-order phase is representative of the steady-state turnover of the enzyme and becomes most pronounced at the absorption maximum (367 nm) of the most intense chromophoric species, IACoA. The k_{cat} value calculated from this progress curve (0.24 s^{-1}) is precisely equal to that predicted under an identical experimental conditions (0.28 s^{-1}). The experimental data at 367 nm have been analyzed by a single exponential plus a zero-order rate equation (solid line).

Effect of $FcPF_6$ Concentration on $1/\tau_1$ and $1/\tau_2$. From the kinetic traces in Figure 4 (left panels), it is evident that, when the aging time reaches 5 s, the amplitudes of the absorption changes attain maxima at all wavelengths. Given the microscopic rate constants for the reductive half-reaction involving IPCoA (Johnson & Srivastava, 1993), it can be calculated that, within this time, the reaction between 1 μM MCAD–FAD and 25 μM IPCoA attains equilibrium with X, and about 74% of the total enzyme is converted into X. By maintaining this aging time, we investigated the effects of $FcPF_6$ concentrations (under pseudo-first-order conditions, i.e., [$FcPF_6$] >> [X]) on the fast and slow relaxation rate constants at 415 nm. As shown in Figure 4 (right panels), the fast relaxation rate constant increases linearly as a function of the $FcPF_6$ concentration (Figure 4, right panel A), whereas the slow relaxation rate constant shows a hyperbolic dependence on the $FcPF_6$ concentration (Figure 4, right panel B). From a linear regression analysis of the data from Figure 4 (right panel A), the slope and intercepts were found to be 0.54 ± 0.01 μM^{-1} s^{-1}, and 2.68 ± 1.98 s^{-1}, respectively. The data from Figure 4 (right panel B) were analyzed by a hyperbolic dependence (with an offset) of $1/\tau_2$ on $FcPF_6$. The $1/\tau_2$-(max), $1/\tau_2$(min), and $K_{0.5}$ were calculated to be 7.20 ± 1.55 s^{-1}, 0.50 ± 1.8 s^{-1}, and 15.13 ± 8.30 μM, respectively.

According to the model presented for the MCAD catalyzed oxidative half reaction (see the Discussion), the enzyme (in the form of X) must form a Michaelian complex with $FcPF_6$ before electron transfer can occur. Realizing that the complex between X and $FcPF_6$ cannot be determined directly by conventional physical techniques due to its short lifetime, we decided to utilize MCAD–FAD (as a putative analogue of X) to detect its interaction with $FcPF_6$. Unfortunately, no signal of interaction between these species could be obtained either by absorption spectroscopy or by circular dichroic spectrometry during titration of 10 μM MCAD–FAD with increasing concentrations of $FcPF_6$ (up to 3 mM) (data not shown). However, a K_m for $FcPF_6$ could be determined to be 2.86 μM during the MCAD-catalyzed reaction in the presence of 100 μM IPCoA (data not shown). Since we are uncertain of the relationship between this K_m value and the microscopic parameters of our overall kinetic model, we have not utilized it for any mechanistic deductions.

DISCUSSION

A comparative investigation of the spectral changes observed via rapid-scanning stopped-flow spectroscopy, coupled with transient kinetic analysis via the sequential mixing stopped-flow method involving both butyryl CoA and IPCoA as enzyme substrates, has allowed us to delineate the microscopic pathway for the MCAD-catalyzed oxidative half-reaction. These investigations have been greatly aided by our prior understanding of the reductive half reaction (Johnson & Srivastava, 1993), as well as by some happenstance spectral properties of the reactants and intermediates during the course of reaction, as summarized here: (1) The rate of formation of the intermediary species X far exceeds the rate of its disappearance during the reductive half-reaction, under conditions where [S] >> [MCAD–FAD] (Schopfer et al., 1988; Johnson & Srivastava, 1993). Hence, X could be populated as a metastable intermediate by appropriately selecting the aging time during the sequential mixing stopped-flow experiments. (2) The extinction coefficients of oxidized and reduced $FcPF_6$ are considerably lower than those of the other chromophoric species, viz., MCAD–FAD, X, IACoA, etc. Consequently, the absorption signals due to the reduction of $FcPF_6$ did not contribute substantially (except at 367 nm; see Figure 3, left panels) during the initial turnover of the enzyme at different wavelengths. (3) The changes in the absorption signals involving butyryl CoA and IPCoA are entirely different, despite the fact that both of these substrates follow a common mechanistic pathway during catalysis.

Changes in the Electronic Structures of Flavin and CoA Derivatives during the Oxidative Half-Reaction. Given that X possesses the spectral properties of the reduced flavin and the highly conjugated reaction product (Johnson & Srivastava, 1993), its reaction with $FcPF_6$ is expected to ultimately produce oxidized flavin (presumably via the formation of a flavin semiquinone intermediate). This expectation is clearly met when X generated by butyryl CoA is allowed to react with $FcPF_6$. As is evident from the data in Figure 3 (left panels), the absorbance at all wavelengths increases as a function of time, but in the opposite sequence from what is observed during the MCAD–FAD + butyryl CoA reaction (data not shown). The increase in absorption during the "burst" phase conforms to a single-exponential rate law at all wavelengths, and the amplitudes of the total absorption changes during the "burst" phase are quantitatively accountable for the oxidation of $FADH_2$ (present in X) to FAD. These facts suggest that, although the oxidation of $FADH_2$ to FAD might proceed via formation of a flavin semiquinone intermediate, the latter presumably is not detectable due to its extremely short lifetime (see below).

Unlike the reaction of butyryl CoA generated X with $FcPF_6$, the complementary reaction involving IPCoA generated X with $FcPF_6$ produces a complex pattern of absorbance changes at different wavelengths (Figure 4, left panels). Clearly, the origin of such complexity lies in the chromophoric nature of the intermediate/product generated during the course of the reaction involving IPCoA as the substrate. One of the major noticeable differences in the kinetic pattern, while utilizing this latter substrate, is the biphasic nature of the reaction progress. At both 450 and 415 nm, the increase in absorbance ($1/\tau_1$ = 22–24 s^{-1}) is followed by a slow decrease ($1/\tau_2$ = 5.5–5.7 s^{-1}) in absorption. However, at 367 nm, a lag phase (equivalent to the time regime of the fast phase at the above wavelengths) is followed by a slow burst (increase) in absorption, with $1/\tau_2 = 4.8\ s^{-1}$. At 367 and 415 nm, the slow phase is followed by a zero-order phase (albeit more pronounced at 367 nm) due to steady-state turnover of the enzyme (see the Results section). It should be pointed out that it is merely a coincidence that at 367 nm both butyryl CoA and IPCoA dependent reactions produce a zero-order, steady-state phase; in the case of butyryl CoA, this phase is given by the difference in the extinction coefficient between oxidized and the reduced $FcPF_6$ (decrease in absorption), whereas in the case of IPCoA it is due to the formation of the intense chromophoric species, IACoA (increase in absorption).

Since at 450 nm the amplitude change during $1/\tau_1$ (ΔA_{450} = 0.040, when the aging time is 5 s) is comparable to that expected for the oxidation of $FADH_2$ to FAD (ΔA_{450} = 0.034, based on the calculation that 2.2 μM X is produced under our experimental conditions), it attests to the fact that the events occurring during $1/\tau_1$ precede those occurring during $1/\tau_2$. Furthermore, given that $1/\tau_2$ measured at 367 nm (increase in absorbance) is comparable to those $1/\tau_2$'s measured at 415 and 450 nm (decrease in absorbance), and that the time regime of the lag phase (at 367 nm) precisely coincides with those of the $1/\tau_1$ phases (at 415 and 450 nm), this suggests that the electronic structural changes during these phases exhibit different absorption properties at different wavelengths.

Just what are the electronically different forms of flavin and CoA derivatives that predominate during the $1/\tau_1$ and $1/\tau_2$ phases of the oxidation reaction? In attempting to answer this question, we considered two possibilities to account for the two relaxation times and the trend in absorption changes at different wavelengths: (1) The oxidation of reduced flavin in X by $FcPF_6$ results in the formation of a (red) flavin semiquinone during $1/\tau_1$, which is fully oxidized during the second ($1/\tau_2$) slow step: (2) The reduced flavin of X is first

$$\mathrm{X(FADH_2,IACoA^*) + Fc_{ox} \rightleftharpoons \rightleftharpoons E(FADH_{sq},IACoA^*) + Fc_{red}} \quad (4)$$

(with Fc_{ox} above the equilibrium arrows and $E(FAD,IACoA^*) + Fc_{red}$ below)

oxidized via two consecutive (albeit fast) transfers of electrons to $FcPF_6$ during $1/\tau_1$, followed by conversion of the conjugated IACoA structure to normal IACoA during the $1/\tau_2$ phase:

$$\mathrm{X(FADH_2,IACoA^*) + \mathit{n}Fc_{ox} \rightleftharpoons \rightleftharpoons E(FAD,IACoA^*)\text{–}\mathit{n}Fc_{red} \rightleftharpoons E(FAD,IACoA)\text{–}\mathit{n}Fc_{red}} \quad (5)$$

Of these two possibilities, the formation of semiquinone during the $1/\tau_1$ phase is discarded in light of the following corroborating evidence: (1) The reaction of X (produced by butyryl CoA) with $FcPF_6$ results in a single exponential burst (increase) in absorbance at all wavelengths, and the amplitude of absorption changes is equal to that predicted for the complete oxidation of $FADH_2$ (present in X) to FAD. Since under our experimental conditions the concentration of $FcPF_6$ exceeds that of X, it is unlikely that during the single-exponential (burst) phase flavin semiquinone would accumulate as a stable species, and it would not oxidize to FAD. (2) The extinction coefficient of the (red) flavin semiquinone at 367 nm is higher than that of fully oxidized flavin (Gorelick et al., 1985), and thus an increase followed by a decrease in absorption at these wavelengths would be expected for the two sequential electron-transfer reactions. This is contrary to our experimental findings. (3) The reaction of X (produced by IPCoA) with

$FcPF_6$ at 450 nm yields an increase ($1/\tau_1$) followed by a decrease ($1/\tau_2$) in absorbance, and the magnitude of $1/\tau_2$ is equal to the single-exponential increase in absorbance at 367 nm. This is contrary to what is predicted for the formation of a (red) semiquinone species (Gorelick et al., 1985). In addition to these, the kinetic arguments (see below) also exclude the possibility of accumulation of flavin semiquinone as a metastable intermediate during the course of the electron transfer reaction. It should be emphasized, however, that the semiquinone formation must occur during the transfer of an electron from $FADH_2$ to the single electron acceptor species, $FcPF_6$. The only argument we offer at this point is that such an intermediary semiquinone has a short lifetime and, thus, is not detectable during our present experimental protocol.

Can our experimental data be explained according to the model of eq 5 [i.e., the oxidation of $FADH_2$ precedes the adjustment of the highly conjugated structure of IACoA (found in X; absorption maximum 400 nm) to that of normal IACoA]? Although this possibility appeared attractive to us initially, we soon realized that the experimental data does not conform to this model either. The following arguments are noteworthy in this context: (1) Despite a very low difference in the extinction coefficient between X and those of the oxidized versus reduced flavin species (Johnson & Srivastava, 1993), the observed absorption changes during both the $1/\tau_1$ and $1/\tau_2$ phases are extensive at 415 nm (see Figure 4, left panels). (2) The oxidation of $FADH_2$ (present in X) by $FcPF_6$ is not likely to yield an increase followed by a decrease in absorption in the 450-nm region. (3) The oxidation of $FADH_2$ (present in X) by $FcPF_6$ cannot be expected to result in a lag phase during the time regime of $1/\tau_1$ (observed at other wavelengths). These facts lead us to propose that the oxidation of $FADH_2$ (of X) by $FcPF_6$ yields the colored (MCAD–FAD*–IACoA**) complex during the $1/\tau_1$ phase, which slowly collapses to a normal colorless (MCAD–FAD–IACoA) complex:

$$\mathrm{X(FADH_2,IACoA^*)} + n\mathrm{Fc_{ox}} \rightleftharpoons \rightleftharpoons \mathrm{E(FAD^*,IACoA^{**})}\text{–}n\mathrm{Fc_{red}} \rightleftharpoons \underset{\text{(colorless)}}{\mathrm{E(FAD,IACoA)}}\text{–}n\mathrm{Fc_{red}} \quad (6)$$

(colored)

Note that this latter sequence is the reverse of that observed by us previously (Johnson et al., 1992) and is explicitly demonstrated by the RSSF data for the interaction of MCAD–FAD with IACoA (Figure 2).

Although the quantitative prediction in absorption changes at individual wavelengths is difficult due to complex overlaps in the spectral pattern, some qualitative assertions are noteworthy: (1) The absorption at 450 nm due to the MCAD–FAD*–IACoA** colored complex is about 10% higher than that found within the MCAD–FAD–IACoA colorless complex (compare the first and the last spectra of Figure 2A). Hence, an increase followed by a decrease in absorption at 450 nm (as observed experimentally; Figure 4, left panels) can only be explained for the formation and decay of the colored complex. (2) In the 420- and 360-nm regions (Figure 2B), the resultant absorption changes are positive and negative, respectively. Thus, an unexpectedly high increase and decrease in absorption at 415 nm during the reaction of IPCoA generated X with $FcPF_6$ are once again explainable for the formation and decay of the MCAD–FAD*–IACoA** colored complex during the $1/\tau_1$ and $1/\tau_2$ phases, respectively. Further support for the formation and the decay of the colored complex comes from the negative absorption peak (at 360 nm) of the enzyme–IACoA complex (Figure 2B) and an expected increase in the absorption at 367 nm due to the oxidation of $FADH_2$ (present in X) by $FcPF_6$; these absorption changes (opposite in magnitude) can cause a lag phase at 367 nm during the time regime of $1/\tau_1$ (Figure 4, left panels). The slow increase in absorption at 367 nm during the $1/\tau_2$ phase is consequently due to isomerization of the MCAD–FAD*–IACoA** colored complex to the MCAD–FAD–IACoA colorless complex. Hence, in the light of the spectral properties of the chromophoric intermediate, the electronic structural changes during the course of the oxidative half reaction have been found to be in accord with the model in eq 6.

Rapidity of the Electron-Transfer Reaction. The linear dependence of $1/\tau$ (in the case of butyryl CoA, Figure 3, right panel), as well as $1/\tau_1$ (in the case of IPCoA), on $FcPF_6$ concentration up to 400 μM (Figure 4, right panel A) suggests a bimolecular (second-order) reaction between X and $FcPF_6$, presumably arising from the collision between these two species. However, the absorption signals responsible for the $1/\tau$ (in the case of butyryl CoA) or $1/\tau_1$ (in the case of IPCoA) phase originate from the oxidation of $FADH_2$ and not from the interaction between X and $FcPF_6$; this latter aspect is supported by the lack of detectable absorption or CD signal changes upon the incubation of 10 μM MCAD–FAD with up to 3 mM $FcPF_6$ (data not shown). Thus, the "apparent" second-order reaction profiles in Figure 3 (right panel) and Figure 4 (right panel A) must originate as a result of the coupled reaction between X and $FcPF_6$:

$$\mathrm{X(FADH_2,IACoA^*)} + n\mathrm{Fc_{ox}} \underset{k_{-1}}{\overset{k_1}{\rightleftharpoons}} \mathrm{X(FADH_2,IACoA^*)}\text{–}n\mathrm{Fc_{ox}} \underset{k_{-2}}{\overset{k_2}{\rightleftharpoons}} \mathrm{E(FAD^*,IACoA^{**})}\text{–}n\mathrm{Fc_{red}} \quad (7)$$

According to the model of eq 7, an obligatory complex between X and $FcPF_6$ is formed before the onset of the electron transfer events. If the association/dissociation reaction involving X and $FcPF_6$ limits the overall relaxation process, the observed relaxation rate constant ($1/\tau$ or $1/\tau_1$) would exhibit a linear dependence (as observed experimentally) on the $FcPF_6$ concentration, irrespective of whether the absorption signal for reaction progress comes from the X–$FcPF_6$ complex or from the oxidized flavin (which is formed subsequent to the complex formation step). It should be pointed out that rapid electron-transfer reactions are not unusual in biological electron transferring systems [for a review, see Moser et al. (1992)]. The unimolecular rate constants for the transfer of electrons between protein-bound cofactors (separated by a 3–5-Å distance) often exceed 10^{10} s^{-1} (Moser et al., 1992). At this time, we cannot predict the rate of electron transfer between enzyme-bound $FADH_2$ and $FcPF_6$ due to the lack of information about the distance separating these species on the enzyme molecule. However, on the basis of our kinetic data, we can justify that the electron transfers in our case must at least be 1000 s^{-1} in order to exhibit a linear dependence of $1/\tau_1$ on $FcPF_6$ concentration. This assertion is based on the approximation of the pseudo-first-order rate constant for the reaction of X (generated by IPCoA) with $FcPF_6$ (400 μM) to be 225 s^{-1} (Figure 4, right panel A), which should be at least 4–5-fold lower than the subsequent electron transfer rate (k_2 in eq 8).

The model of eq 7 is analogous to those proposed for a number of enzyme/protein systems where "long-range" electron-transfer mechanisms are encountered (Chapman et al., 1984; Adzamli et al., 1981; Navarro et al., 1991). In fact, all of the theories of electron-transfer reactions proposed so far rely on the "static" juxtaposition of donor and acceptor

molecules at a fixed distance (Tiede et al., 1993; Meyer et al., 1993). From this point of view, we did not consider an explanation for our kinetic data based on alternative models that would exclude complex formation between X and $FcPF_6$.

It should be pointed out that the present model (eqs 5–7) relies on the fact that the stoichiometric ratio of $FcPF_6$ to enzyme subunit (which contains one $FADH_2$ molecule) must at least be 2 ($n \geq 2$). Such a stoichiometric ratio would not demand dissociation and reassociation of $FcPF_6$ (1-electron acceptor) repeatedly (two times) during the oxidation of $FADH_2$ to FAD. The sequential association and dissociation of $FcPF_6$ would have resulted in two (instead of one) relaxation times during the course of 2-electron oxidation of $FADH_2$. This is particularly important since the rate-limiting step during the $1/\tau_1$ phase appears to be the association "on rate" between enzyme and $FcPF_6$. A higher stoichiometric ratio of $FcPF_6$ to the enzyme subunit is not unlikely since a number of "unspecific" ligands (of hydrophobic nature) are known to bind at more than one site on the protein molecule (Dixon & Webb, 1979; Z. X. Wang & D. K. Srivastava, unpublished results).

Microscopic Pathway for the MCAD-Catalyzed Oxidative Half-Reaction. A cumulative account of all of the experimental results and the foregoing discussions lead us to propose a comprehensive model for the MCAD-catalyzed dehydrogenation reaction:

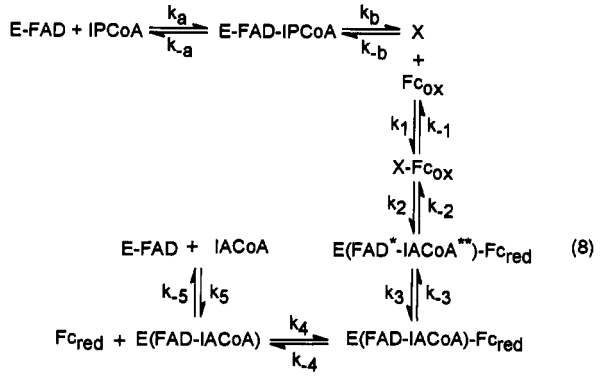

(8)

In this model, the dissociation of the reduced $FcPF_6$ has been considered to occur prior to the dissociation of IACoA, although the opposite sequence would not affect our kinetic analysis. Given that the overall reaction of X with $FcPF_6$ is consistent with only two observed relaxation rate constants, it follows that the other microscopic steps of eq 8 are fast. Since the absorption signals during $1/\tau_1$ and $1/\tau_2$ have been established to arise from the oxidation of $FADH_2$ (of X) to FAD and the isomerization of the MCAD–FAD*–IACoA** colored complex, the microscopic pathway starting from the reaction of X with Fc_{ox} of eq 8 can be reduced to the following form:

$$X + Fc_{ox} \underset{k_{21}}{\overset{k_{12}}{\rightleftharpoons}} E(FAD^*\text{–}IACoA^{**}) \underset{k_{543}}{\overset{k_3}{\rightleftharpoons}} E(FAD)_{total} \quad (9)$$

$E(FAD)_{total}$ represents all of the enzyme species (i.e., E–FAD–IACoA–Fc_{red}, E–FAD–IACoA and E–FAD) which possess the spectral properties of oxidized flavin. The magnitudes of these species are the functions of Fc_{red} and IACoA concentrations, and they can be quantitatively represented by the corresponding microscopic rate constants of eq 8. The aggregated rate constants in terms of the microscopic parameters of eq 8 can be given as follows (Laidler & Bunting, 1973):

$$k_{12} = k_1 \quad (10)$$

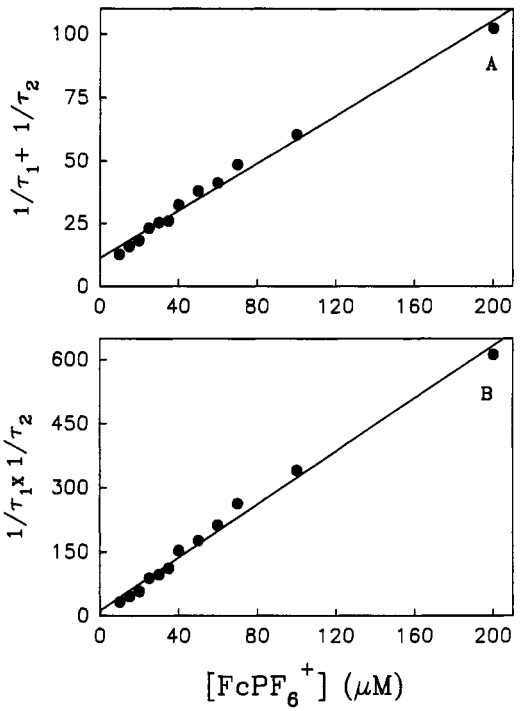

FIGURE 5: Dependence of $(1/\tau_1 + 1/\tau_2)$ and $(1/\tau_1)(1/\tau_2)$ on $FcPF_6$ concentrations. The solid lines are calculated for the linear dependence of these constants on $FcPF_6$ concentration. The slopes and intercepts derived for the best fit of experimental data are 0.47 ± 0.02 μM^{-1} s^{-1} and 11.25 ± 1.17 s^{-1} for $(1/\tau_1 + 1/\tau_2)$ versus $FcPF_6$ plot and 3.11 ± 0.1 μM^{-1} s^{-2} and 13.01 ± 7.5 s^{-2} for $(1/\tau_1)(1/\tau_2)$ versus $FcPF_6$ plot.

$$k_{21} = k_{-1}k_{-2}/(k_2 + k_{-2}) \quad (11)$$

$$k_{543} = k_{-3}/((1 + (K_R/[Fc_{red}]) + (K_I K_R/[IACoA][Fc_{red}])) \quad (12)$$

where K_R and K_I are the dissociation constants of the E(FAD–IACoA)–Fc_{red} (k_{-4}/k_4) and E(FAD–IACoA) (k_{-5}/k_5) complexes respectively. Without making any assumptions, the relationships between the relaxation rate constants and the (aggregated) kinetic parameters of eq 9 can be given by (Bernasconi, 1976):

$$1/\tau_1 + 1/\tau_2 = k_{12}[Fc_{ox}] + k_{21} + k_3 + k_{543} \quad (13)$$

$$(1/\tau_1)(1/\tau_2) = k_{12}[Fc_{ox}]\,(k_3 + k_{543}) + k_{21}k_{543} \quad (14)$$

Figure 5A,B shows the plots of $1/\tau_1 + 1/\tau_2$ and $(1/\tau_1) \times (1/\tau_2)$ as functions of the $FcPF_6$ concentration, respectively. As predicted by eqs 13 and 14, these plots exhibit linear dependence on $FcPF_6$ concentration. By linear regression analysis of the data from Figure 5A, the slope and intercept have been found to be 0.47 ± 0.02 μM^{-1} s^{-1} and 11.25 ± 1.17 s^{-1}, respectively, and the corresponding parameters from the data from Figure 5B have been found to be 3.11 ± 0.01 μM^{-1} s^{-2} and 13.01 ± 7.50 s^{-2}, respectively. On the basis of relationships given in eqs 10–14, the individual (aggregated) rate constant from the slope and intercept values of Figure 5A,B can be extracted as follows: the slope and intercept of this figure are denoted as A and B, respectively (Bernasconi, 1976).

$$k_{12} = \text{slope A} = 0.47\ \mu M^{-1}\ s^{-1}$$

$$k_{21} = \text{intercept A} - (\text{slope B}/\text{slope A})$$
$$= 11.25 - (3.11/0.47) = 4.63\ s^{-1}$$

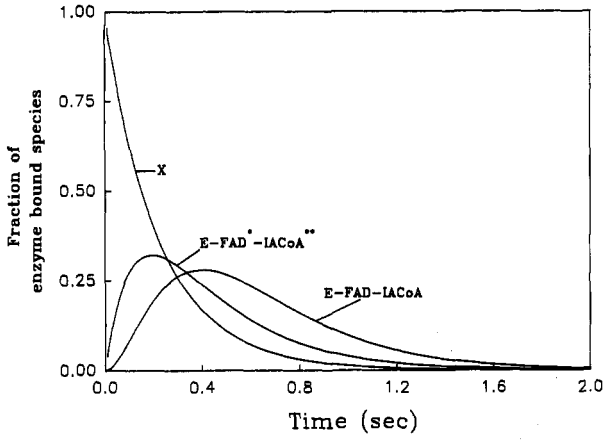

FIGURE 6: Numerical simulation results for the MCAD–FAD/IPCoA + $FcPF_6$ reaction for the kinetic model of eq 8. The time courses for the disappearance of X and the appearance of E–FAD•–IACoA•• (colored) and E–FAD–IACoA (colorless) are shown. The concentrations of X and $FcPF_6$ were taken to be 0.74 and 10 μM, respectively, for the simulated traces presented herein. The y-axis represents the fractional concentration of these species. The rate constants utilized in these simulations are as follows: $k_1 = 0.47\ \mu M^{-1}\ s^{-1}$; $k_{-1} = 4.62\ s^{-1}$; $k_2 = 1000\ s^{-1}$; $k_{-2} = 1.0\ s^{-1}$; $k_3 = 6.0\ s^{-1}$; $k_{-3} = 0.5\ s^{-1}$; $k_4 = 4.62\ s^{-1}$; $k_{-4} = 0.47\ \mu M^{-1}\ s^{-1}$; $k_5 = 1000\ s^{-1}$; $k_{-5} = 100\ \mu M^{-1}\ s^{-1}$.

$$k_{543} = \text{intercept B}/k_{21}$$
$$= 13.01/4.62 = 2.81\ s^{-1}$$

$$k_3 = \text{intercept A} - (k_{21} + k_{543})$$
$$= 11.25 - (4.62 + 2.81) = 3.81\ s^{-1}$$

Having determined these (aggregated) rate constants, we proceeded to translate them into the microscopic rate constants of the comprehensive model of eq 8. In this pursuit, we realized that both k_{21} and k_{543} are complex functions of the various rate and equilibrium constants, some of which are not known independently. For example, k_{21} contains a term from the equilibration of X with $FcPF_6$, as well as ones from the forward (k_2) and reverse (k_{-2}) electron-transfer steps (eq 8). Of these, at the most a lower limit of k_2 can be set to be 1000 s^{-1} (see argument above). Hence, unless the magnitude of either k_{-1} or k_{-2} is known independently, the individual microscopic parameters cannot be obtained. Admittedly, our inability to determine the dissociation constant of the enzyme–$FcPF_6$ complex has hampered such quantitation. The parameter k_{543} is far more complex than k_{21} due to the additional involvement of concentration terms, which cannot be ascertained a priori. It follows that, despite our attempt to determine the aggregated rate constants of the simplified eq 9, there is no analytical solution of our experimental data. Hence, recourse was made to numerical simulation of the model of eq 8. Figure 6 shows the time-dependent changes in concentrations of different intermediary species during the course of the oxidative half-reaction involving 0.74 μM X (generated upon prior incubation of 1 μM MCAD–FAD and 25 μM IPCoA for 5 s) and 40 μM $FcPF_6$. The rate constant selected during this simulation has been appended to the legend forFigure 6. The simulated curve for the formation and decay of the MCAD–FAD•–IACoA•• colored complex is consistent with the two relaxation rate constants ($1/\tau_1 > 1/\tau_2$) with magnitudes equal to those found experimentally. Furthermore, $1/\tau_1$ and $1/\tau_2$ exhibit linear and hyperbolic dependence on $FcPF_6$ concentration, respectively. Such dependencies are qualitatively similar to our experimental data in Figure 4 (right panels). This attests to the internal consistency of our model.

Prior to this work, a number of groups had investigated the oxidative half-reaction of MCAD catalysis utilizing octanoyl CoA reduced enzyme and ETF–FAD as the electron acceptor (Hall et al., 1979; Hall & Lambeth, 1980; Gorelick et al., 1985; Gorelick & Thorpe, 1986). In their most elaborate studies, Gorelick et al. (1985) found multiphasic kinetics during the oxidative half-reaction, the two fast phases of which were assigned to the formation and decay of the flavin semiquinone species. At this point, we offer no explanation for this discrepancy, particularly since our substrate and electron acceptors are different from those used by Gorelick et al. (1985). Does this imply that the microscopic pathway for the dehydrogenation reaction involving octanoyl CoA substrate is different from that obtained in the presence of either butyryl CoA or IPCoA? Alternatively, octanoyl CoA reduced enzyme produces an equilibration mixture of X and other species, but only X participates in the oxidative half-reaction. Under this condition, the reaction with ETF–FAD would yield relaxation times not only due to the reaction between X and ETF–FAD but also due to the equilibration between X and its cognate species. Similar arguments can be valid for the reaction where $FcPF_6$ (instead of ETF–FAD) has been utilized as an electron acceptor (Lehman & Thorpe, 1990). Are these differences due to the nature of substrates or due to experimental design? Clearly our understanding of the substrate dependent influence on the MCAD catalyzed reaction must await further experimental results.

REFERENCES

Adzamli, I. K., Davies, D. M., Stanley, C. S., & Sykes, A. G. (1981) *J. Am. Chem. Soc. 103*, 5543–5547.

Auer, H. E., & Frerman, F. E. (1980) *J. Biol. Chem. 255*, 8157–8163.

Beckmann, J. D., & Frerman, F. F. (1985) *Biochemistry 24*, 3913–3921.

Beinert, H. (1963) *The Enzymes*, 2nd ed., Vol. 3, pp 447–466, Academic Press, New York.

Bernasconi, C. F. (1976) *Relaxation Kinetics*, Academic Press, New York.

Betts, G. F., & Srivastava, D. K. (1991) *J. Theor. Biol. 151*, 155–167.

Chapman, S. K., Davies, D. M., Vuik, C. P. J., & Sykes, A. G. (1984) *J. Am. Chem. Soc. 106*, 2692–2696.

Crane, F. L., & Beinert, H. (1956) *J. Biol. Chem. 218*, 717–731.

Dixon, M., & Webb, E. C. (1979) *Enzymes*, 3rd ed., pp 332–467, Academic Press, New York.

Frerman, F. E., Miziorko, H. M., & Beckman, J. D. (1980) *J. Biol. Chem. 255*, 11192-11198.

Ghisla, S., Thorpe, C., & Massey, V. (1984) *Biochemistry 23*, 3154–3161.

Gorelick, R. J., Schopfer, L. M., Ballou, D. P., Massey, V., & Thorpe, C. (1985) *Biochemistry 24*, 6830–6839.

Hall, C. L., & Lambeth, J. D. (1980) *J. Biol. Chem. 255*, 3591–3595.

Hall, C. L., Lambeth, J. D., & Kamin, H. (1979) *J. Biol. Chem. 254*, 2023–2031.

Ikeda, Y., Okamura-Ikeda, K., & Tanaka, K. (1985) *J. Biol. Chem. 260*, 1311–1325.

Johnson, J. K., & Srivastava, D. K. (1993) *Biochemistry 32*, 8004–8013.

Johnson, J. K., Wang, Z., & Srivastava, D. K. (1992) *Biochemistry 31*, 10564–10575.

Knoop, F. (1904) *Beitr. Chem. Physiol. Pathol. 6*, 150.

Laidler, K. J., & Bunting, P. S. (1973) *The Chemical Kinetics of Enzyme Action*, 2nd Ed., Oxford Press, London.

Lehman, T. C., & Thorpe, C. (1990) *Biochemistry 29*, 10954–10601.

Lehman, T. C, Hale, D. E, Bhala, A., & Thorpe, C. (1990) *Anal. Biochem. 186*, 280-284.

McFarland, J. T., Lee, M., Reinsch, J., & Raven, W. (1982) *Biochemistry 21*, 1224-1229.
Meyer, T. E., Zhao, Z. G., Cusanovich, M. A., & Tollin, G. (1993) *Biochemistry 32*, 4552–4559.
Moser, C. C., Keske, J. M., Warncke, K., Farid, R. S., & Dutton, P. L. (1992) *Nature 355*, 796–802.
6–802.
Murfin, W. W. (1974) Ph.D. Dissertation, Washington University, St. Louis, MO.
Navarro, J. A., Gleason, F. K., Cusanovich, M. A., Fuchs, J. A., Meyer, T. E., & Tollin, G. (1991) *Biochemistry 30*, 2192–2195.
Pohl, B., Raichle, T., & Ghisla, S. (1986) *Eur. J. Biochem. 160*, 109–115.
Savitzsky, A., & Golay, M. J. E. (1964) *Anal. Chem. 36*, 1627–1639.
Schopfer, L. M., Massey, V., Ghisla, S., & Thorpe, C. (1988) *Biochemistry 27*, 6599-6611.
Thorpe, C., Matthews, R. G., & Williams, C. H., Jr. (1979) *Biochemistry 18*, 331–337.
Tiede, D. M., Vashishta, A.-C., & Gunner, M. R. (1993) *Biochemistry 32*, 4515–4531.
Wang, R., & Thorpe, C. (1991) *Biochemistry 30*, 7895–7901.